Available online at www.sciencedirect.com
SCIENCE DIRECT®
Continental Shelf Research 25 (2005) 1097–1114
CONTINENTAL SHELF RESEARCH
www.elsevier.com/locate/csr

The structure of the coastal density front at the outflow of Long Island Sound during spring 2002

A.R. Kirincich*, D. Hebert

Graduate School of Oceanography, University of Rhode Island, Narragansett, RI 02882, USA

Received 1 March 2004; received in revised form 1 December 2004; accepted 21 December 2004

Abstract

South of the eastern end of Long Island (Montauk Point) along the Eastern U.S. coast, a coastal density front forms between the buoyant outflow plume of the Long Island Sound (LIS) and the denser shelf waters offshore. During a 2-day cruise in April 2002, measurements of the density and velocity structure of this front were obtained from high-resolution CTD and ADCP data. Transects show the front intersecting the bottom inshore of the 30 m isobath and shoaling offshore. Variability in the location of the front is small offshore of the 40 m isobath, yet tidal excursions of the front along the bottom are significant (5 km) inshore of this depth.

The frontal structure of the LIS plume was similar to observations of bottom-trapped coastal density fronts and shelf break fronts. A coastal jet in the along front direction was the main feature of the mean velocity field and was found to be in thermal wind balance with the mean density field. Stronger than expected offshore velocities near the surface, most likely a result of wind forcing, were the only exception to these similarities. In addition, analysis of temperature and salinity gradients along isopycnals gives evidence of secondary cross-frontal circulation and detachment of the bottom boundary layer. Characteristics of the LIS plume are used to evaluate recent analytical models of bottom-trapped coastal density fronts and bottom-advected plume theory, finding good agreement.

Keywords: Density fronts; Buoyant plumes; USA; Middle Atlantic Bight; Long Island

1. Introduction

On the continental shelf, one of the principal forcing mechanisms for coastal and shelf circulation is the localized inflow of buoyancy (Yankovsky and Chapman, 1997). Associated with freshwater discharge into coastal estuaries, these sources form buoyant plumes separated from denser shelf waters by a sharp density front. In many instances, the buoyant plume spans the water column as it flows onto the shelf. Yankovsky and Chapman (1997) categorized different types of

*Corresponding author. College of Atmospheric and Oceanic Sciences, Oregon State University, Corvallis, OR 97331, USA.
E-mail addresses: akirinci@coas.oregonstate.edu (A.R. Kirincich), hebert@gso.uri.edu (D. Hebert).

0278-4343/$ - see front matter © 2005 Elsevier Ltd. All rights reserved.
doi:10.1016/j.csr.2004.12.014

plumes based on their contact with the bottom topography and described two characteristic types. Bottom-advected plumes occupy the entire water column at depths greater than the depth at which the plume enters the shelf, or the inflow depth. Here, the behavior of the plume and location of the front are controlled by advection in the bottom boundary layer. A shelf-break front is an example of this type of frontal structure. The second type, surface-advected plumes, are known to initially spread radially from the inflow site and exist primarily above shelf waters, only remaining in contact with the bottom at the coast. This type forms a small coastal current downstream of the source region (Garvine, 1987). Yankovsky and Chapman (1997) cite the Niagara River plume in Lake Ontario as an example of this second type.

The primary difference between these two main types of buoyant plumes and associated fronts results from the strength of the plume's interaction with the bottom. Work by Wright (1989) and Chapman and Lentz (1994) has documented the important interaction between density advection in the bottom boundary layer and the velocity field. Chapman and Lentz (1994) found that feedback between these processes could lead to the trapping of the front–bottom intersection by the bottom boundary layer. When the out-flowing plume reaches the bottom, Ekman forcing in the bottom boundary layer causes the offshore advection of the density gradient. This offshore advection occurs until the outflow no longer reaches the bottom, and onshore advection offshore of the front opposes further offshore motion (Chapman and Lentz, 1994; Pickart, 2000). At this critical depth, the front is trapped. If the out-flowing current does not reach the bottom, this interaction will not take place and the front–bottom intersection will remain onshore (Yankovsky and Chapman, 1997). Thus, the degree to which the along-front velocity field interacts with the bottom determines the structure and location of the associated coastal density front.

A number of observations and model studies of these types of coastal fronts exist. Barth et al. (1998), Pickart (2000), and Houghton and Visbeck (1998) all described the density and velocity structure of the shelf break front in the Middle Atlantic Bight. The authors found a mature front, in thermal wind balance, having a surface intensified along-front jet with substantial vertical shear reducing velocity with depth to a slight opposing velocity at the base of the front. Barth et al. (1998) reported a reversal in the flow direction across the foot of the front in the across-front direction implying convergence at the front, and mixing across the frontal interface. Using dye injection, Houghton and Visbeck (1998) found that upwelling along isopycnals occurred on both sides of the front. Here, the secondary circulation across the front has been observed using beam attenuation results (Barth et al., 1998) or dye tracers (Houghton and Visbeck, 1998). More recently, Pickart (2000) showed that the signature of this cross-frontal circulation was present in two-dimensional sections of temperature. Similar primary and secondary velocity structure was found in a modeling effort by Chapman and Lentz (1994). In addition to the characteristics mentioned above, their model study described a general off-shore flow existing mostly shoreward of the front resulting in a second area of possible convergence.

Model studies and observations have also been made of smaller scale fronts along coastal buoyant plumes. The model results of Garvine (1987) found that shallow inflows tend to have a pool region near the outflow with a smaller coastal current forming further downstream. Munchow and Garvine (1993), observed a similar structure south of Delaware Bay as a results of the outflow of buoyant waters from the bay. The plume and current, called the Delaware Coastal Current (DDC), matches the surface trapped plume type described by Yankovsky and Chapman (1997). Munchow and Garvine also cited the similarities of the DCCs dynamics with the model results of Chapman and Lentz (1994).

With observations and model studies such as these in mind, a number of authors have developed scaling criteria to both predict the plume type based on their inflow conditions and characterize the dynamics of the plume. Yankovsky and Chapman (1997) developed criteria based solely on the buoyant plume's outflow conditions to predict the plume type, the trapping depth, and the forcing mechanism of the plume and front. Lentz

and Helfrich (2002) improved on these efforts by developing scaling parameters to describe flows along a sloping boundary.

A coastal density front regularly occurs in the area south of Montauk Point and Block Island as a result of buoyancy forcing (Fig. 1). Flowing south and west around Montauk Point, the buoyant plume originating from the Long Island Sound (LIS) encounters the ambient shelf waters in the area south of Montauk Point, with a front forming at the boundary. The sea surface temperature (SST) results of Ullman and Cornillon (1999) infer that the front is relatively constant in location. They found SST fronts in the area predominantly in a band centered near the 50 m isobath (or closer to shore in the summer). In addition, the plume is known to span the water column as it passes south of Montauk Point (Bowman and Esaias, 1981). However, little else is known about the dynamics of this particular front.

This study aims to describe the density and velocity structure of the coastal density front formed by the outflow of the Long Island Sound south of Montauk Point. The measurements used in this analysis are described in Section 2, while Sections 3 and 4 give descriptions of the general hydrography and the mean velocity fields found. A comparison of these results with previous observations along with an evaluation of the scaling theories of Yankovsky and Chapman (1997) and Lentz and Helfrich (2002) using the results is presented in Section 5. Section 6 summarizes the results of this study.

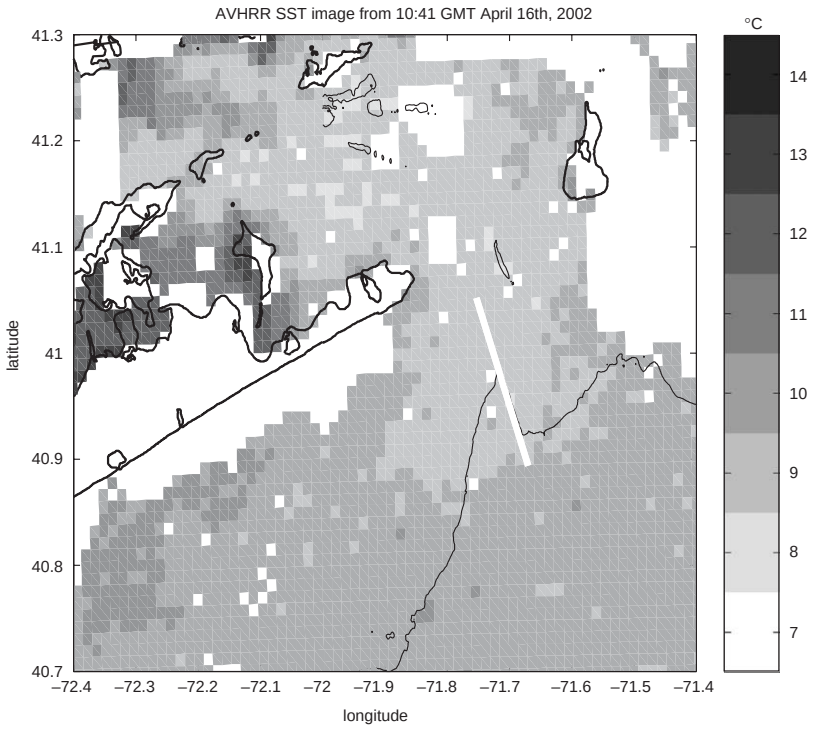

Fig. 1. Advanced Very High Resolution Radar (AVHRR) image of sea surface temperature (SST) in the study area on April 16, 2002. The outline of Montauk Point, the eastern tip of Long Island, is shown as well as Block Island located to the east. North of these two points is the Block Island Sound (BIS), while south is the study area. White denotes regions masked because of cloud coverage. The image shows a plume of cool water leaving the Long Island Sound (LIS) through its eastern end and flowing east into Block Island Sound (BIS). Here the plume turns south, flowing into the study area and appears to turn to the west. The front of interest here is located at the boundary between the plume and shelf waters to the south and east. The main transect line occupied during the study is shown as the thick white line. The 50 m isobath (thin black line) is included for reference. SST data courtesy of D. Ullman.

2. Description of experiment

Measurements of temperature, salinity, transmissivity, and water velocity were obtained on the continental shelf south of Montauk Point during a 2-day cruise to the study area on April 15–16, 2002 (yearday 105–106) using the R/V Connecticut. During daylight hours, CTD measurements obtained using an Acrobat, a towed undulating body made by Sea Sciences, and water velocity measurements obtained using a 600 Hz Workhorse ADCP from RDI were made along a transect line from 41°03.115′N, 71°45.202′W to 40°53.631′N, 71°40.205′W (Fig. 1). The Acrobat carried a Seabird Sealogger SBE25 CTD and a WET Labs C-STAR transmissometer as payload. The ADCP, mounted on the hull of the Connecticut, sampled at 1 Hz, with a depth interval of 1 m starting at 5.5 m below the water surface. This combination of instruments was used to produce two-dimensional vertical sections along the 20 km transect line approximately every 2 h with vertical and horizontal resolutions of 1 m and $\frac{1}{2}$ km, respectively. Five transect were made on the 15th with the remaining six obtained on the 16th. This particular transect line was chosen to be aligned with other in-water components of the Front Resolving Observational Network with Telemetry (FRONT) Project (Codiga, 2005). In addition to the Acrobat towing during daylight hours, a larger scale CTD survey was performed overnight using a Seabird SBE 9+, adding a larger scale view of the hydrographic conditions present in the study area. ADCP transects of the main transect line were made during the large scale CTD station survey as well. A detailed account of the preliminary processing of all data collected can be obtained in Kirincich (2003) or Kirincich and Hebert (2002).

During the cruise period, the frontal structure was observed over three full tidal cycles. The detailed structure of the front can be clearly seen with these profiles, and a comparison of multiple transects identifies movement of, or changes in the structure of the front as well as its tidal motions over the period sampled. Moderate atmospheric conditions existed during the study period. Using NOAA's nearby offshore data buoy (#44025), winds during the cruise were found to be generally from the south-southwest and moderate, ranging from 9 m/s on the 15th to 4 m/s on the 16th. Significant wave heights during the time period ranged from 1 to 1.5 m.

3. General hydrography

The general hydrography of the waters south and east of Montauk Point is described here using the combination of AVHRR imagery, a representative transect made by the Acrobat, and the wider area CTD station survey. The large-scale CTD survey results and AVHRR image put the 2D sections made using the Acrobat in the context of the larger scale hydrographic structure existing during the study period.

An AVHRR image of sea surface temperature (SST), obtained the morning of the 16th, shows the location of the buoyant plume in the study area (Fig. 1). The plume, with surface temperatures of 7.5–8.5 °C, fills most of the Block Island Sound and continues south through the opening between Montauk Point and Block Island. The transect line occupied lies in an approximately north-northwest to south-southeast orientation and is located mostly inside the SST plume (Fig. 1). Waters offshore of the plume and to the south of the transect line are a degree or more warmer.

The Acrobat transect collected during maximum ebb tide at Montauk Point was chosen as the representative transect that best highlights the hydrography of the area and the general structure of the front during the cruise period (Fig. 2). This transect's temperature section has a surface front at the same location as the AVHRR SST image seen earlier (Fig. 1). However, the results show that this surface feature is not part of the greater frontal stratification seen below the surface in the salinity and density sections (Fig. 2). A comparison of temperature, salinity, and density finds that salinity is the major contributor to the structure of the density field. The locations of isopycnals are most similar to isohaline locations throughout the transect, and the sharpest gradients in both are co-located. With the front defined as the region of highest horizontal change of σ_t, a clearly defined

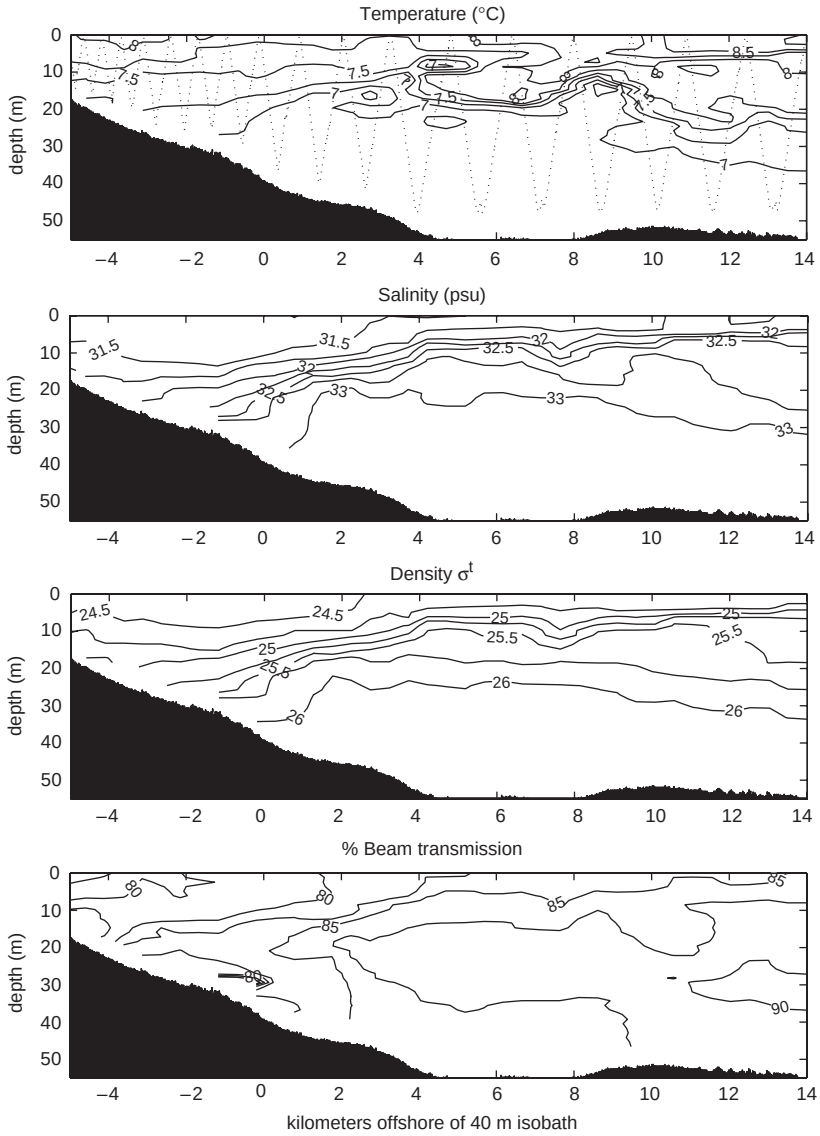

Fig. 2. Representative sections of temperature, salinity, density, and beam transmission show the general hydrographic conditions present during the cruise. These two dimensional vertical sections show hydrographic conditions in a coordinate system of distance (km) offshore of the 40 m isobath by depth (m) below the surface. The Acrobat CTD track line is overlaid on the top profile for reference.

front with a frontal stratification of $d\sigma_t/dz = 0.1\,kg\,m^{-4}$ can be seen shoaling offshore from 25 m depth at 0 km offshore of the 40 m isobath to 5 m depth at 5 km offshore of the 40 m isobath. Thus, the front does not intersect the surface within the study area in this representative transect, nor any of the remaining 10 transects made.

Transmissivity is generally lowest throughout the water column within the inshore end of the plume region while increasing offshore along the surface (Fig. 2). Transmissivity is also low along the bottom within the plume and offshore of the plume along the sloping bathymetry with the lowest values occurring where the front intersects

the bottom. These high turbidity areas are believed to result from large tidal flows along the bottom, which will be discussed later.

In this study it is assumed that a specific density surface lies in the middle of the frontal gradient and can adequately represent the front over time. To find this isopycnal, the horizontal derivative of density (σ_t) with respect to distance along the transect (x), or $d\sigma_t/dx$, was calculated for all 11 density sections to establish the location of the intensified horizontal density gradient. The locations of the maximum horizontal derivative for each depth above a threshold (found by inspection as $0.25\,kg\,m^{-3}$ per 500 m) were compiled to mark the location of the highest horizontal gradients within each section. The mean value of σ_t at the location of these maxima in all transects ($\sigma_t = 25.25$) was used as the density surface of the frontal interface.

Comparing the locations of this isopycnal in all transects illustrates the vertical stability of the front over the course of the study period (Fig. 3). Within the area measured, the mean frontal interface is located at 5 m depth offshore and slopes downwards moving inshore to 20 m depth at the 35 m isobath. The vertical standard deviation of the depth of the front ranges from a maximum of 6 m at 5 km offshore of the 40 m isobath to a minimum of 3 m at 0 and 12 km offshore. Inshore of the 30 m isobath, significant

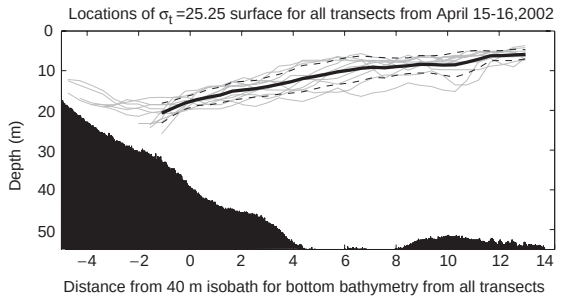

Fig. 3. The locations of the density surface marking the mean frontal interface in all transects (light lines). The isobath of the front–bottom intersection (found by extrapolation) varied over the course of a tidal cycle. This location was near the 30 m isobath near low tide at Montauk Point, but inshore of the 20 m isobath at high tide. The mean frontal interface depth (solid black line) and its standard deviations (dashed black lines) for all transects is overlaid.

vertical and horizontal variability of the frontal interface location was observed. The excursions of the front in this area were at the same period as, and in phase with, the M2 tide at Montauk Point. Thus, these excursions are believed to be a result of tidal forcing. The maximum tidal excursion of the front's intersection with the bottom is greater than 5 km along the transect line, corresponding to more than 12 vertical meters as a result of the slope of bathymetry in the area. Using the magnitude of along-transect measured velocities in this region, a similar horizontal movement can be inferred.

The large-scale CTD survey conducted the night between the two Acrobat towing periods highlights the larger scale structure of the buoyant plume in the study area (Fig. 4). This wider view of the study area puts the data collected along the transect line into the context of the region-wide hydrographic features. The depth of the $\sigma_t = 25.25$ isopycnal reveals the slope of the front in the study area. Inshore, it sinks to 25 m depth and intersects the bottom on the seaward edge of the plume. In general, the front is deepest in the area of the 35–40 m isobaths (all three north–south ship track transects), but over the course of a tidal cycle the front–bottom interface can shoal considerably. This shoaling can be seen at station A (Fig. 4). Viewing station A and B together illustrates the spatial and temporal variability of the plume. Sampled consecutively, the front is found inshore at A but was not found at B. In a second sampling of the middle transect 5 h later (not shown), the frontal interface was not present at either station A or B, and both had similar well-mixed vertical profiles characteristics of the plume waters.

4. Velocity results

The mean velocity field during the 2-day period was determined using velocity measurements collected along the transect line by the R/V Connecticut's ADCP. After removing tidal velocities as described below, the mean velocity field was computed from the average of the residual velocities from all transects. A thermal wind balance for the study period is examined using the mean velocity section and the average density

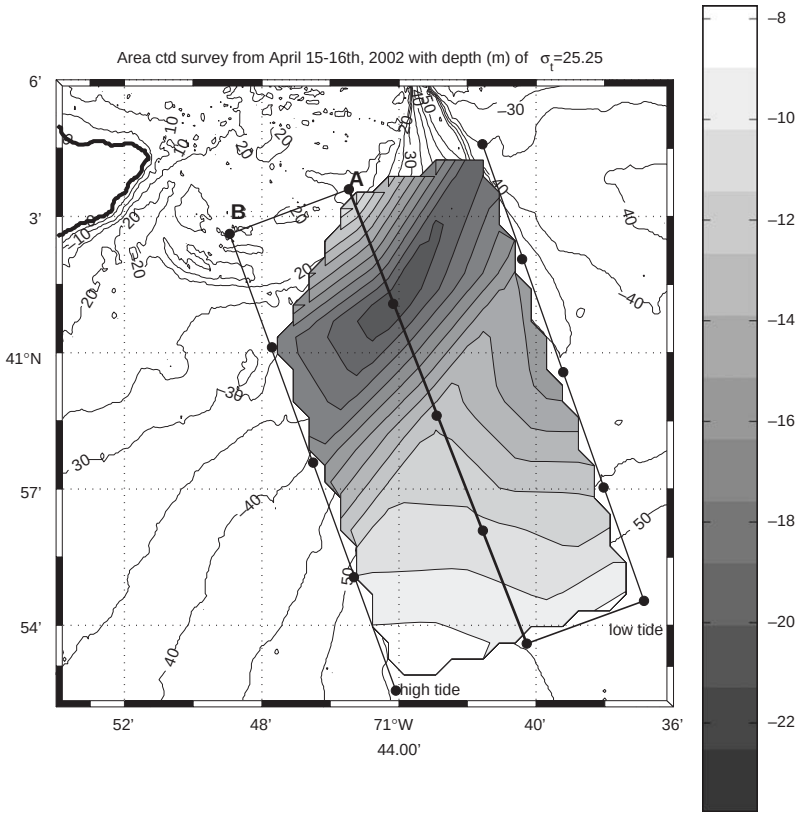

Fig. 4. Large scale CTD survey results displayed as the depth of the $\sigma_t = 25.25$ isopycnal, calculated to be at the frontal interface. The ship track is also included here (starting at the northeast station) to highlight time differences between station samplings. The approximate location of the ship during low and high tide at Montauk Point is noted as well. Waters at station B were less dense than the frontal interface density, indicating the front intersected the bottom to the south and east of this station.

field. The mean velocity field is subsequently rotated into a coordinate system aligned with the front for further analysis.

4.1. Calculating the mean velocity field

The mean velocity field was determined using all velocity measurements collected along the main transect line during the 2-day period. Here, the measured water velocities were assumed to be composed simply of a mean component plus time varying components, or:

$$V_{measured} = V_{mean} + V_{tidal} + V_{random}, \quad (1)$$

where V_{tidal} represents water velocities caused by the M2 tidal constituent and V_{random} represents all remaining time varying components. The M2 constituent was the only tidal frequency considered here due to the short record length and intermittent frequency of sampling. However, this tidal component is known to cause the dominant tidal velocity in the area (Ianniello, 1981; Ullman and Codiga, 2004). Therefore, assuming the M2 tidal velocities are large compared to the average random components, an average of $V_{measured} - V_{tidal}$ taken over the entire cruise gives an estimate of the mean velocity field present.

Tidal velocities were obtained using a least squares fit to a spatially varying current and an oscillating component having the period of the M2 tide. Velocity measurements taken along the main transect line were first interpolated onto an evenly

spaced 2D grid (depth by along-transect distance). For each station, the closest ensembles from each ADCP transect, if within 0.5 km of the station, were used to create a time series of velocity. For each depth interval at each station, the tidal velocities and ellipses were calculated using the least squares harmonic analysis of Foreman (1978).

The explained variance, a measure of how well the mean and tidal-varying M2 components explain the observed velocities, is found as:

$$r^2 = 1 - \frac{\overline{(V_{timevarying} - V_{tidal})^2}}{\overline{(V_{timevarying})^2}}. \quad (2)$$

The computed mean and tidal velocities accounted for most of the measured velocity in many parts of the transect, with a few notable exceptions. In the along-transect direction, results were low only in the top few meters of the measured water column south of 6 km offshore (Fig. 5). In the across-transect direction, areas of poor tidal fit existed in the middle of the water column inshore and near the top of the measured area at 6 km offshore. In both directions, the largest area of best fit was centered along the bottom at 1 km offshore and 30 m depth, just below the approximate location of the mean frontal interface. Here, this simple fit accounted for nearly all of the measured velocity.

A comparison of the maximum tidal velocities in the along-transect and across-transect directions illustrates the range of tidal forcing along the transect line (Fig. 6). Generally, tidal velocities decrease moving offshore in the along-transect direction except for a small area of increase at 1 km offshore and 20–30 m depth. This decrease is also present in the offshore half of the across-transect maximum tidal velocities. However, in the corresponding inshore half, tidal velocities are highest in the region around 1–2 km offshore just below the frontal interface. Inshore of the front, tidal velocities decrease to a minimum in the across-transect direction. An area of strong tidal velocities exists below the front in both directions (Fig. 6).

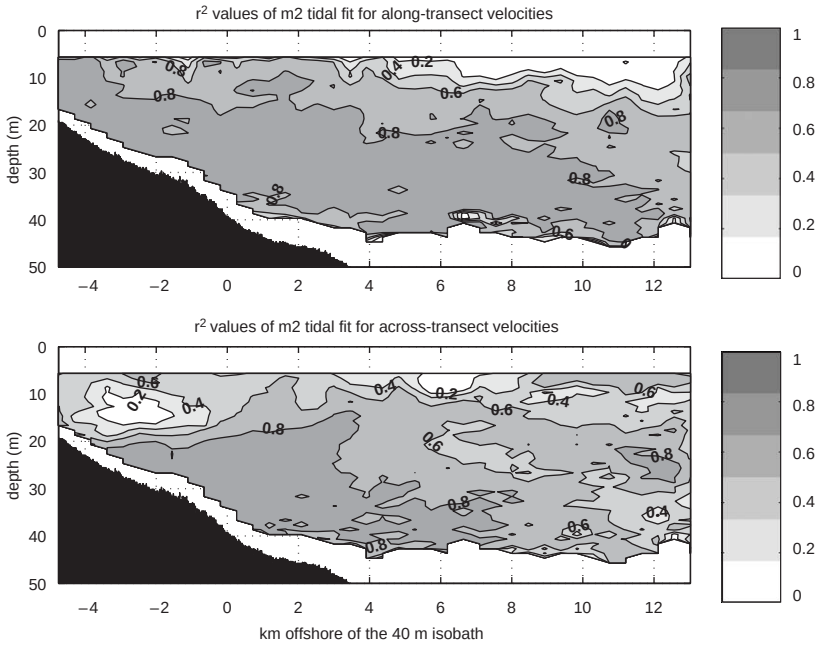

Fig. 5. Results of the r^2 analysis for along-transect (top) and across-transect (bottom) velocities. These panels show the fraction of the total variance at each station and depth accounted for by the mean and tidal components of the measured velocities. The majority of the along-transect velocities are explained by the mean and M2 tidal velocities, except for the area near the surface and offshore. Values are also high near the bottom inshore in the across-transect direction.

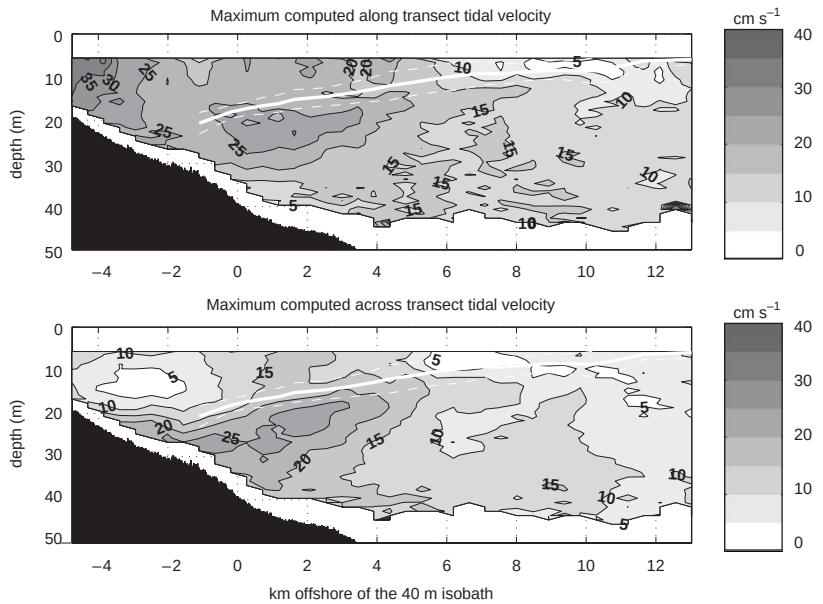

Fig. 6. Maximum computed tidal velocities for both the along-transect (top) and across-transect (bottom) direction. Generally, tidal velocities decrease moving offshore in both sections, except for an area of strong tidal velocities in the across-transect direction at 1 km offshore. The frontal interface (solid white line) and associated standard deviation (dashed white lines) are included for reference.

Given the sparseness of ADCP sampling, computed tidal ellipses were compared to those calculated from available HF radar surface current data for the same time period and location, reported in Ullman and Codiga (2004) (not shown here), for a check of accuracy. While discrepancies existed offshore where tidal velocities from both sources are small, M2 tidal ellipses from both sources generally had similar orientations and amplitudes along the transect line. This additional check adequately validates the results of the tidal fits used in the computation of the mean velocity field.

The standard deviation of the detided velocities gives additional insight into the uncertainty in the mean velocity. In general, if mean detided velocities are less than their standard deviations, or noise velocity, they are not significantly different than zero. Large noise velocities were found near the surface in the along-transect direction (Fig. 7), while lower values of $5\,\mathrm{cm\,s^{-1}}$ or less exist below this area and over most of the across-transect profile. Based on the distribution of the standard deviation of the noise velocity seen here, mean detided velocities less than $5\,\mathrm{cm\,s^{-1}}$ throughout the majority of the both profiles may not be significantly different from zero. In contrast, between 5 and 7 m depth in the along-transect direction, mean detided velocities must be greater than the $20\,\mathrm{cm\,s^{-1}}$ noise velocity found in order to be significant (Fig. 7). Finally, there are a number of regions, such as 10–20 m depth at 2 km inshore of the 40 m isobath and at mid-depth at 10–12 km offshore, where time varying velocities must be small as small tidal velocities where found in addition to low standard deviations.

Removing the computed tidal velocities from the measured velocities and averaging gives the mean velocity sections in the along and across transect direction. Before rotating these velocities into a coordinate system referenced to the front, a thermal wind balance calculation is performed using the across-transect velocity section.

4.2. Thermal wind balance

The thermal wind balance describes the relationship between the vertical shear of the velocity

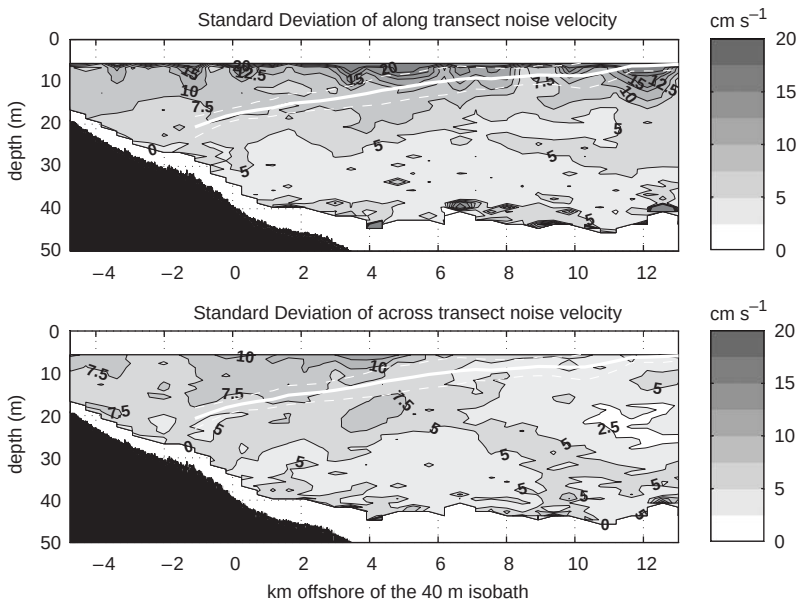

Fig. 7. Standard deviation of the noise velocity. Computed velocity components (shown in Fig. 9) are not significantly different than zero where the standard deviation of the noise velocity is larger than the mean detided velocity or the tidal fits. The highest noise velocities are found in the top meters of the along transect direction.

normal to the transect and the horizontal density gradient along the transect line for a geostrophic flow, or:

$$\frac{\partial u}{\partial z} = \frac{g}{\rho_o f}\frac{\partial \rho}{\partial y} \tag{3}$$

where $g = 9.81\,\mathrm{m\,s^{-2}}$, $\rho_o = 1025\,\mathrm{kg\,m^{-3}}$ is a reference density, and the Coriolis parameter, f, is estimated at $9.5 \times 10^{-5}\,\mathrm{s^{-1}}$. To find if this balance exists here, the mean density field was used to determine the theoretical velocity shear in the across-transect direction. Comparing this result with the vertical shear of the mean across-transect velocity gradients illustrates whether the density and velocity structures are in thermal wind balance.

A comparison of theoretical and measured vertical shear shows good agreement with similar magnitudes and distributions (Fig. 8). In the section of theoretical vertical shear, the approximate location of the front is marked by the highest shear values. This region is located in a line shoaling offshore from the 30 m isobath to 5 m depth (Fig. 8). A similar feature, both in location and magnitude is found in the measured velocity shear. Below this area and offshore, much smaller values exist in both the derived and measured shear sections; although the measured shear profile is significantly noisier (Fig. 8). Thus, the across-transect velocity structure seems to be in thermal wind balance with the observed mean density gradients.

4.3. Mean rotated velocity field

For further analysis, the mean velocity profiles were rotated into a coordinate system oriented along and across the front. Since results from the large scale survey showed the transect line's orientation was clockwise (CW) of normal to the front, mean velocity sections were rotated counter-clockwise (CCW) until the structure of the coastal jet disappeared from the across-front direction, minimizing the net transport in this direction. Rotating the coordinate system approximately 20° CCW accomplishes this goal and this new section orientation is referred to here as the along- and across-front directions. The new coordinate

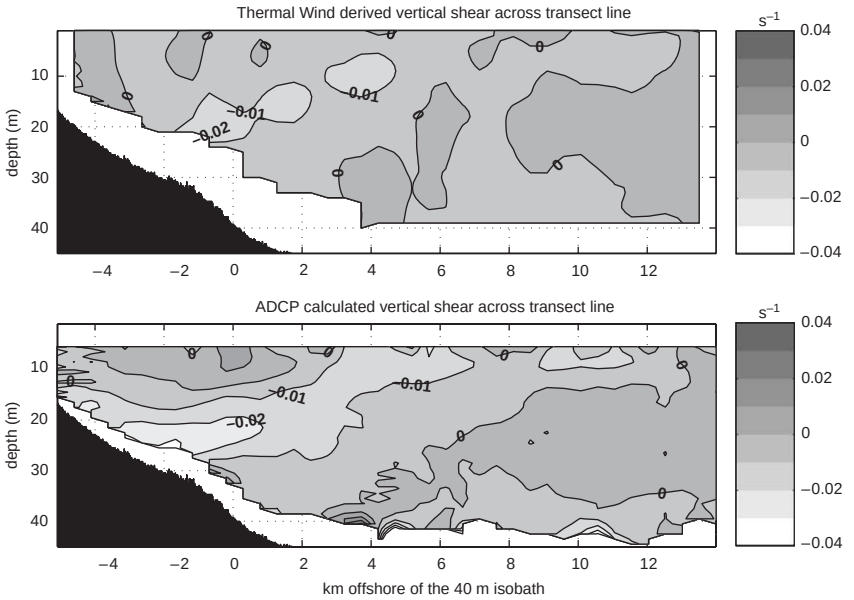

Fig. 8. Thermal wind balance. The velocity shear predicted by the density derived vertical shear (s^{-1}) (top panel) shows small values throughout most of the water column with the exception of the area located between 2 and 5 km offshore. Here an elevated region is found which parallels the location of the mean frontal interface (Fig. 3). The vertical shear of the mean across transect velocity profile (lower panel) has a similar distribution as well as the same order of magnitude.

system is used throughout the remainder of this analysis.

In the rotated coordinate system, a robust coastal jet exists in the along-front direction, flowing towards the southwest with maximum velocities of 35–40 cm s^{-1} (Fig. 9). Across-front velocities are small (5–10 cm s^{-1}) offshore below 10 m depth. Velocities in this direction decrease with depth and become weakly onshore below and offshore of the stronger velocities above (Fig. 9). Above 10 m depth in the across-front direction, a significant vertical shear still exists with offshore velocities increasing within the top 5 m of the measured area to 20 cm s^{-1}. A potential cause of this shear will be discussed later.

The core of the coastal jet lies just inshore and above the frontal interface in the along-front profile (Fig. 9). A smearing of the mean velocities could be present since water velocities were averaged by location, yet are dependent on the location of the frontal interface. However, the small standard deviation of the frontal interface indicates the possible velocity smear zone offshore of the 30 m isobath is also relatively small. Consequentially, velocity smearing does not seem to be a factor. In fact, the frontal interface is located just above the region of highest tidal velocities. The lower edge of the jet extends well below the mean frontal interface and reverses direction close to the bottom. In contrast, across-front velocities change direction just below the front, except for a small area of rather weak onshore flow (less than the noise velocity for the area) existing at 20 m depth on both sides of the base of the front (Fig. 9). Within the water column (10–30 m depth) between 10 and 12 km offshore, an area of slightly higher water velocities (5–10 cm s^{-1}) exists directed onshore and east (negative).

5. Discussion

The coastal jet and frontal structure observed here is clearly similar to the trapped coastal density fronts described by Chapman and Lentz (1994) and the shelf-break front observations of Barth et al. (1998) and Pickart (2000), as well as

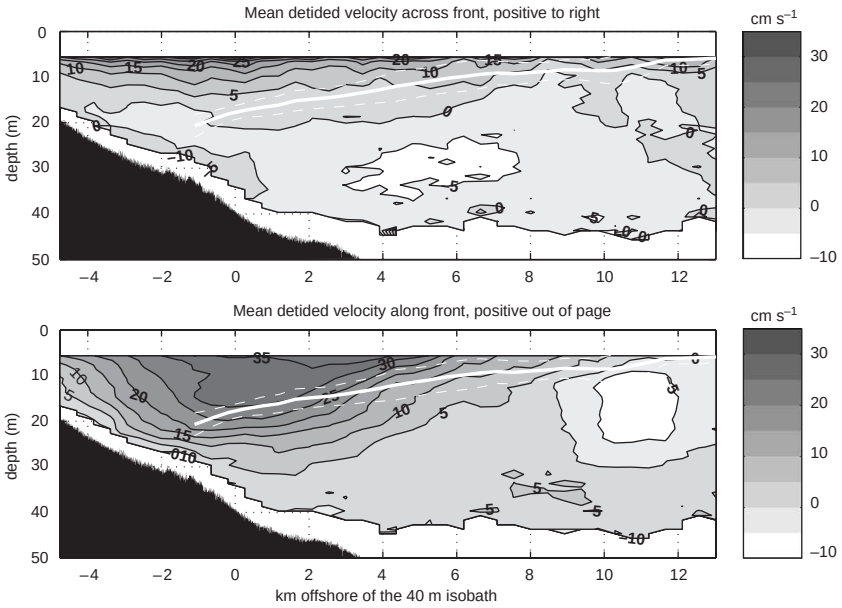

Fig. 9. Mean detided velocities rotated into across-front (upper panel) and along-front (lower panel) directions. The frontal interface and standard deviation locations are overlaid for reference.

other observations of plume fronts (Munchow and Garvine, 1993). Many of the characteristic features of trapped density fronts described earlier are visible in the velocity structure of the LIS plume front. A coastal jet, in thermal wind balance with the mean density field, is seen in the along-front direction with significant vertical shear. Velocities at the base of the front in the along-front direction are near zero, if not slightly opposing the along-front jet. The offshore flows in the plume below 10 m depth in the across-front direction are of similar magnitude and direction as the examples of shelf break observations and model studies given earlier (Barth et al., 1998; Chapman and Lentz, 1994; Pickart, 2000). However, above this region much stronger velocities exist.

A number of topics are reserved for discussion here. The magnitude and vertical shear of velocities in the top 10 m of the across-front velocity section are not seen in the modeling results of Chapman and Lentz (1994) or the observations of Barth et al. (1998), and their cause is discussed first. Next, secondary, cross-frontal circulation is a known feature of bottom-trapped density fronts. We look for evidence of this at the LIS plume front following the isopycnal analysis method of Pickart (2000). In addition, the theory of Chapman and Lentz (1994), Yankovsky and Chapman (1997), and Lentz and Helfrich (2002) all imply that plumes on the scale of the LIS outflow can and do form coastal trapped density fronts like those found at a shelf break region. While we have documented the many similarities between the LIS plume and trapped density fronts here, this point is investigated further using parameters developed by Yankovsky and Chapman (1997) and Lentz and Helfrich (2002) to estimate the type of plume and front present. The estimated trapping depth of the front is identified using Yankovsky and Chapman's (1997) theory, and the LIS plume is categorized based on the non-dimensional parameters of Yankovsky and Chapman (1997), and the plume propagation speeds of Lentz and Helfrich (2002). Finally, the implications of the large tidal excursions of the foot of front are discussed.

5.1. Anomalous surface velocities

The region of strong offshore velocities located above 10 m depth in the across-front direction (Fig. 9) cannot be simply accounted for by the

general circulation of a typical bottom-trapped coastal density front. One obvious possible explanation for the large vertical shear and significant noise velocities in this area is wind forcing. Wind velocities for the days immediately preceding sampling in the region were $9\,m\,s^{-1}$ from the south-southwest and decreased throughout the study period to $4\,m\,s^{-1}$. Analysis of the along-transect velocity sections shows stronger offshore surface velocities occurred more frequently on the first cruise day, further supporting this possibility.

With these points in mind, it is of interest to find if offshore Ekman transport could account for these increased surface velocities. The average wind direction during the 2-day period crossed the transect line counter-clockwise of normal, yet was approximately normal to the rotated velocity direction. The maximum wind stress τ ($N\,m^{-2}$) following Large and Pond (1981) is:

$$\tau_s = \rho_a C_f U^2, \tag{4}$$

where $\rho_a = 1.25\,kg\,m^{-3}$, U is the wind speed, and C_f is the neutral 10 m drag coefficient found by Large and Pond (1981) for wind speeds from 4 to $11\,m\,s^{-1}$ to be 0.0012. The calculated wind stress is used to predict the maximum Ekman transport from:

$$M_{ek} = \frac{\tau}{\rho_o f}. \tag{5}$$

The maximum Ekman transport, perpendicular to the direction of the wind, is parallel to the across-frontal velocity direction. Dividing this transport by the depth of the mixed layer (10 m as shown in Fig. 2) gives an average velocity of $16\,cm\,s^{-1}$. These results, of the same order of magnitude as the offshore across frontal velocity between 5 and 10 m depth (Fig. 9), indicate wind forcing could have accounted for the surface offshore flows seen. This result is similar to that reported by Shearman and Lentz (2003) for the Coastal Mixing and Optics experiment. There, the only discrepancy in the thermal wind balance between the mean flow and the density structure was also caused by Ekman transport near the surface.

5.2. Evidence of secondary circulation

Upwelling along the frontal isopycnals is a characteristic feature of bottom-trapped fronts. The feature is an indication of the detachment of the bottom boundary layer from the foot of the front. This phenomenon has been described in the model studies of Gawarkiewicz and Chapman (1992) and Chapman and Lentz (1994) as well as observations of a dye tracer study reported by Houghton and Visbeck (1998). Following the isopycnal analysis technique developed by Pickart (2000), we look for evidence upwelling along isopycnals at the LIS plume front.

In high-gradient regions such as fronts, significant along-isopycnal mixing is expected. However, if water parcels are being actively pumped along isopycnals by a detached bottom boundary layer, lateral along-isopycnal gradients of temperature and salinity will be reduced relative to adjacent isopycnal surfaces (Pickart, 2000). Following the method described by Pickart (2000), sections of temperature and salinity were converted to density space and the offshore gradients along isopycnals of each were found. Accumulated temperature and salinity changes were calculated by integrating the absolute value of these off-shore gradients along isopycnals. Converting the resulting sections back to the depth verses offshore distance reference frame gives sections of accumulated change of temperature and salinity (Fig. 10). For the representative transect, both temperature and salinity accumulation show a distinct tongue of minimum accumulation rising from the foot of the front along the path of the main frontal stratification (Fig. 10). This low accumulation region is the signature of a detached bottom boundary layer (Pickart, 2000). Similar results were found for the remaining transect lines collected during the 2-day period, indicating this type of secondary, cross-frontal, circulation does seem to be present at the LIS plume front.

5.3. Trapping depth

Further evidence of the similarities between this plume and a bottom-advected plume can be determined by estimating the trapping depth of

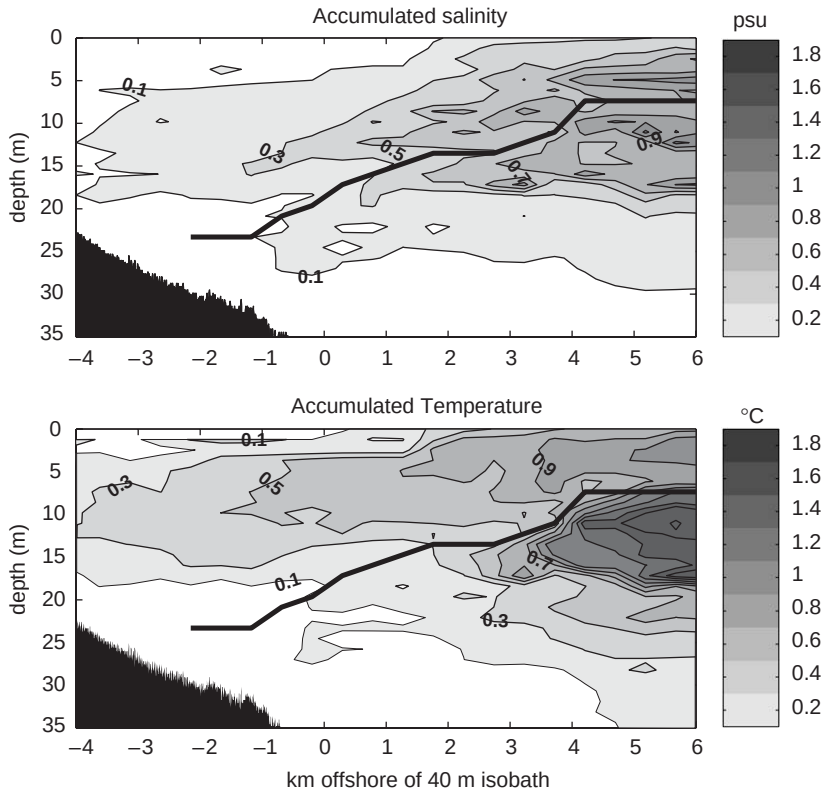

Fig. 10. Accumulated change of salinity (top) and temperature (bottom) of the representative transect following the method of Pickart (2000). The tongue of minimum accumulated temperature and salinity moving up from the foot of the front is the signature of the detachment of the bottom boundary layer and upwelling along isopycnals in the front. The location of the $\sigma_t = 25.25$ isopycnal is overlaid for reference.

the front. Yankovsky and Chapman (1997) found for a bottom-advected plume, the trapping depth of the front can be directly related to the magnitude of flow in the plume and the density difference across the front by:

$$h_B = \sqrt{\frac{2Qf}{g'}}, \tag{6}$$

where h_B is the trapping depth, Q is the plume transport, and reduced gravity g' is given by:

$$g' = \frac{\rho'}{\rho_o} g, \tag{7}$$

where ρ' is the density difference across the front ($1\,\mathrm{kg\,m^{-3}}$). For the LIS plume, a transport of $38,800\,\mathrm{m^3\,s^{-1}}$ was found by integrating the rotated along-frontal velocity inshore of the mean frontal interface. Using these values, the trapping depth, h_B, of the plume originating from the LIS was estimated as 27.5 m. To compare this result with our observations, an estimated bottom intersection depth can be found by extending the mean frontal interface to the bottom (Fig. 3). This results in a bottom intersection at the 26–28 m isobath. The close proximity of these results gives further evidence of the similarities between the LIS plume and a bottom-advected plume. Thus, this front appears to be a bottom-trapped front.

5.4. Evaluation of scaling parameters

Given the observations of the LIS plume front described above and it's similarity to coastal

density fronts observed at the shelf break, it is of interest to see how the parameters developed by Yankovsky and Chapman (1997) and Lentz and Helfrich (2002) categorize the LIS plume and front. Yankovsky and Chapman's criteria are designed to predict the behavior of the plume based solely on its characteristics as it enters the shelf. The two non-dimensional parameters the authors use to characterize plumes are the Rossby (Ro) and the Burger (S) numbers:

$$Ro = \frac{V}{fL} \tag{8}$$

and

$$S = \frac{(g'h_o)^{1/2}}{fL}. \tag{9}$$

Here, V is the velocity of plume waters as they enter the shelf, L is the horizontal width of the gap through which the plume enters the shelf, and h_o is the average depth of this opening.

Divisions between plume types are made using the following non-dimensional equations signifying the horizontal (offshore) length scales of the front–bottom intersection (Y_b), and the front-surface intersection (Y_s):

$$Y_b = \frac{h_o}{sL}\left(\frac{(2Ro)^{1/2}}{S} - 1\right) \tag{10}$$

and

$$Y_s = \frac{2(3S^2 + Ro^2)}{(2S^2 + Ro^2)^{1/2}}. \tag{11}$$

The term ho/sL is a basin specific parameter depending on the bottom slope s.

Plumes with low Burger numbers will be most similar to Yankovsky and Chapman's (1997) bottom-advected plumes except at small Rossby numbers (<0.1). Similarly, plumes having a Burger/Rossby ratio greater than 1.5–2 for Rossby numbers greater than 0.1, or greater than 4 for Rossby numbers less than 0.1, will have features most similar to surface-advected plumes. Results falling between these two types have surface characteristics similar to surface-advected types even though the trapping depth is accurately predicted by bottom-advected plume theory (Yankovsky and Chapman, 1997).

Examining this relationship for the study area using half the opening between Montauk Point and Block Island for the inflow gap, or $L = 12$ km, $h_o = 20$ m, $s = 0.6\,\mathrm{m\,km^{-1}}$ (Codiga, 2005), and an inflow velocity, V_i, of $20\,\mathrm{cm\,s^{-1}}$ (the average of the plume transport, Q, found earlier), these dimensionless parameters are $Ro = 0.17$, and $S = 0.38$. Re-plotting Yankovsky and Chapman's (1997) Fig. 3 using $h_o/sL = 2.77$ (specific to the LIS outflow), the LIS plume falls on the $Y_b = Y_s$ line (Fig. 11). This line serves as the border between the intermediate and bottom-trapped plume types (Yankovsky and Chapman, 1997). Potential error in this result seems most dependent on estimates chosen for the inflow velocity and the width of the gap. Lower inflow rates would decrease the inflow Rossby number, while the use of a larger gap size (if the plume occupies the entire opening between Montauk Point and Block Island, Fig. 1) would decrease both dimensionless numbers. Shifting V_i and L as such moves the LIS location along the $Y_b = Y_s$ line only (Fig. 11). Thus, these approximate values for the LIS plume, following Yankovsky and Chapman (1997), correspond to an intermediate plume having features most closely related to a bottom-advected plume.

Yankovsky and Chapman (1997) developed these criteria using a model bathymetry having a vertical wall inshore to the inflow depth, h_o, and a sloping bottom at depths greater than the inflow depth. More recently, Lentz and Helfrich (2002) have updated these criteria to incorporate a fully sloping boundary. Their new work defines whether buoyancy currents are surface-trapped or slope controlled based on the ratio of two propagation speeds, c_w and c_α, where:

$$c_w = \sqrt{g'h_B} \tag{12}$$

and

$$c_\alpha = \frac{\alpha g'}{f}. \tag{13}$$

In Lentz and Helfrich (2002), the bottom slope is represented by α as opposed to s used previously. Thus, c_w is the propagation speed of the nose of a gravity current along a vertical wall, while c_α is the

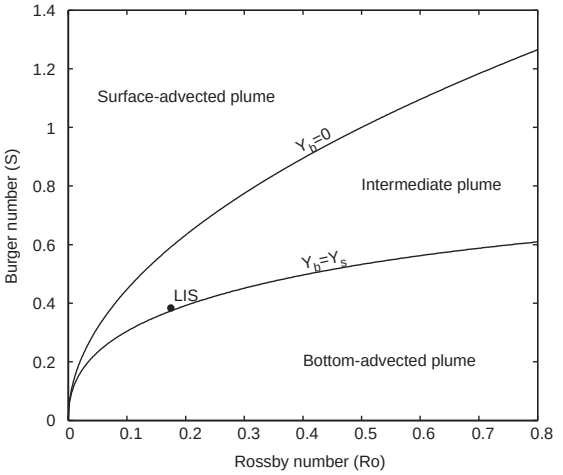

Fig. 11. After Fig. 3 in Yankovsky and Chapman (1997), but with $h_o/sL = 2.77$. Based on the relationship of the Rossby and Burger numbers of the inflow plume, the plume type can be split into the regions seen here. Given an inflow depth (h_o), Yankovsky and Chapman (1997) define the curves dividing the regions based on non-dimensionalized distance scales of the front–bottom intersection (Y_b) and front-surface intersection (Y_s). A surface-advected plume forms when the bottom trapping depth (h_b) is less then the inflow depth (h_o). An intermediate plume is defined as occurring when the theoretical scale of the front's bottom intersection is less than the scale of the front's surface intersection ($Y_b < Y_s$). Similarly, a bottom-advected plume forms when the theoretical bottom intersection scale is greater than the front-surface intersection ($Y_b > Y_s$). The approximate location of this relationship for the LIS plume is marked above.

propagation of the nose in the limit of small bottom slope. If $c_w/c_\alpha \gg 1$, the buoyancy current is surface trapped. If $c_w/c_\alpha \ll 1$ the buoyancy current is slope-controlled or bottom-trapped. Evaluating these propagation speeds for the LIS plume front give $c_w = 0.52\,\mathrm{m\,s^{-1}}$ and $c_\alpha = 0.44\,\mathrm{m\,s^{-1}}$, thus the ratio of c_w/c_α is 1.17. According to these criteria, the LIS plume is an intermediate plume, having characteristics of both types.

In addition, Lentz and Helfrich (2002) define the offshore width of the front, (W_w), as:

$$W_w = \frac{c_w}{f}. \tag{14}$$

Using $c_w = 0.52\,\mathrm{m\,s^{-1}}$, this distance is 5.5 km, much smaller than the horizontal distance covered by the frontal stratification seen here (Fig. 2). However, if the region marked by relatively horizontal isopycnals offshore of 4 km is not included as part of the width of the front, the LIS front width is quite close to the distance estimated following Lentz and Helfrich. In addition, when $c_w/c_\alpha \geqslant 1$, Lentz and Helfrich (2002) found that a recirculating bulge developed near the source. It is thought that the level isopycnals offshore might be part of such a feature.

Overall the scaling parameters of both Yankovsky and Chapman (1997) and Lentz and Helfrich (2002) seem to describe the LIS plume and front well. The trapping depth estimated following Yankovsky and Chapman (1997) accurately predicts the depth of the foot of the front. Both methods also estimate the LIS plume as being a intermediate type plume, although while Yankovsky and Chapman's (1997) method shows it on the border of intermediate plumes and bottom-trapped plumes (Fig. 11), Lentz and Helfrich's (2002) method gives a more intermediate plume. Both methods do quite well given that the location of this study was in close proximity to the inflow of the LIS plume.

5.5. Tidal excursions

The large tidal excursions of the front along the bottom are of further interest as they infer that significant stretching of the frontal interface occurs near the bottom. Tidal velocities in our study were significantly higher then observations of bottom-trapped fronts. For the shelf break front, Barth et al. (1998) measured tidal velocities of 2–15 $\mathrm{cm\,s^{-1}}$ from offshore to onshelf at the shelf break. In our study area tidal velocities were found to be greater then 20–25 $\mathrm{cm\,s^{-1}}$ at the front's intersection with the bottom (Fig. 6). As a result, the horizontal excursions of the front over a tidal cycle is greater than 5 km along the transect line, corresponding to a significant vertical change. If the excursions seen are accurately represented by the two-dimensional profile used, significant stretching and contracting of the frontal gradient must occur.

Tidal advection of a spatial varying plume through the transect line could also cause the isopycnal movement seen in Fig. 3. While this process cannot be disproved completely given the

two-dimensional nature of sampling, as stated earlier, a similar horizontal movement of isopycnals in the along-transect direction can be inferred using the magnitude of the measured velocities. The computed tidal velocities provide additional support as tidal velocities in the across-transect direction within the plume are significantly smaller then mean velocities, and southeast flow consistently occurs in the plume during all parts of the tidal cycle (Kirincich, 2003; Kirincich and Hebert, 2002). Tidal velocities in the plume in the along-transect direction as well as beneath the plume in the across-transect direction are large (Fig. 6), and coincide with the areas of large isopycnal displacement (Fig. 3). Thus, the large isopycnal movement seen over the course of a tidal cycle seems to be a result of tidally forced motion of the front–bottom interface in the along-transect direction, implying that the frontal interface near the bottom stretches and contracts over the course of a tidal cycle. This stretching of isopycnals should lead to a strengthening and narrowing of the frontal interface. Such movements should tend to cause increased mixing of the plume and shelf waters over time. It is unclear what effects stretching of the interface might have on the cross frontal circulation present or the frontal stability in general.

6. Summary

The hydrographic and velocity results from the 2-day cruise to the LIS plume front south of Montauk Point reveal the structure and short-term variability of this coastal density front. The density front intersected the bottom between the 20 and 40 m isobaths and shoaled moving offshore. The coastal jet found in the study area was in thermal wind balance with the density gradient, and resembled that found at typical shelf break fronts. Evidence of cross-frontal circulation and bottom boundary layer detachment at the front–bottom intersection were also found using along-isopycnal gradients of temperature and salinity. High offshore near-surface velocities were found in the plume as well, possibly as a result of surface Ekman transport during the cruise.

The comparison of our results with those found in the literature show the structure of this front has striking similarities to observations and models of bottom-trapped coastal density fronts. The front–bottom intersection of the mean frontal interface matched the trapping depth for bottom-advected plumes given by Yankovsky and Chapman (1997). Although measurements made here were much closer to the source region than the analysis of Yankovsky and Chapman (1997) and Lentz and Helfrich (2002), the good agreement between the results and these authors' criteria for bottom-trapped plume fronts add further support to theory created for these types of coastal buoyancy forcings. However, adding short-term variability to the frontal location, large lateral tidal excursions of the plume and the front–bottom intersection were found here. Possibly the cause of stretching of the frontal isopycnals, this feature is a significant difference between the results found here and models and observations of bottom-trapped coastal density fronts.

References

Barth, J.A., Bogucki, D., Pierce, S.D., Kosro, P.M., 1998. Secondary circulation associated with a shelf break. Geophysical Research Letters 25 (15), 2761–2764.

Bowman, M.J., Esaias, W.E., 1981. Fronts, stratification, and mixing in Long Island and Block Island Sounds. Journal of Geophysical Research 86 (C5), 4260–4264.

Chapman, D.C., Lentz, S.J., 1994. Trapping of a coastal density front by the bottom boundary layer. Journal of Physical Oceanography 24, 1464–1478.

Codiga, D., 2005. Interplay of wind forcing and buoyant discharge off Montauk Point: seasonal changes to velocity structure and a coastal front. Journal of Physical Oceanography, in press.

Foreman, M.G.G., 1978. Manual for tidal currents analysis and prediction. Pacific Marine Science Report No. 78-6. Institute of Ocean Sciences, Sidney, B.C. Canada.

Garvine, R.W., 1987. Estuary plumes and fronts in shelf waters: a layer model. Journal of Physical Oceanography 17, 1877–1896.

Gawarkiewicz, G.G., Chapman, D.C., 1992. The role of stratification in the formation and maintenance of shelf-break fronts. Journal of Physical Oceanography 22, 753–772.

Houghton, R.W., Visbeck, M., 1998. Upwelling and convergence in the Middle Atlantic Bight shelf break front. Geophysical Research Letters 25 (15), 2765–2768.

Ianniello, L.P., 1981. Tidally-induced residual currents in the Long Island and Block Island Sounds. Estuarine Coastal and Shelf Science 12, 177–191.

Kirincich, A., 2003. The structure and variability of a coastal density front. Masters Thesis, University of Rhode Island.

Kirincich, A., Hebert, D., 2002. NOPP front resolving observational network with telemetry (FRONT) project frontal scale hydrographic surveys. GSO Technical Report, reference no. 2002-01.

Large, W.G., Pond, S., 1981. Open ocean momentum flux measurements in moderate to strong winds. Journal of Physical Oceanography 11, 324–336.

Lentz, S.J., Helfrich, K.R., 2002. Buoyant gravity currents along a sloping bottom in a rotating fluid. Journal of Fluid Mechanics 464, 251–278.

Munchow, A., Garvine, R.W., 1993. Dynamical properties of a buoyancy-driven coastal current. Journal of Geophysical Research 98 (C11), 20,063–20,077.

Pickart, R.S., 2000. Bottom boundary layer structure and detachment in the shelfbreak jet of the middle Atlantic bight. Journal of Physical Oceanography 30, 2668–2686.

Shearman, R.K., Lentz, S.J., 2003. Dynamics of mean and subtidal flow on the New England shelf. Journal of Geophysical Research 108 (C8), 3281.

Ullman, D.S., Codiga, D.L., 2004. Seasonal Variation of a coastal jet in the Long Island Sound outflow region based on HF radar and Doppler current observations. Journal of Geophysical Research 109 (C0TS06).

Ullman, D.S., Cornillon, P.C., 1999. Satellite-derived sea surface temperature fronts on the continental shelf off the northeast U.S. Coast. Journal of Geophysical Research 104 (C10), 23459–23478.

Wright, D.G., 1989. On the along shelf evolution of an idealized density front. Journal of Physical Oceanography 19, 532–541.

Yankovsky, A.E., Chapman, D.C., 1997. A simple theory for the fate of buoyant Coastal Discharges. Journal of Physical Oceanography 27, 1386–1401.